Combined processing and mutual interpretation of radiometry and fluorimetry from autonomous profiling Bio-Argo floats: Chlorophyll a retrieval

Xiaogang Xing, André Morel, Hervé Claustre, David Antoine, Fabrizio d'Ortenzio, Antoine Poteau, Alexandre Mignot

Combined processing and mutual interpretation of radiometry and fluorimetry from autonomous profiling Bio-Argo floats: Chlorophyll *a* retrieval

Xiaogang Xing,[1] André Morel,[1] Hervé Claustre,[1] David Antoine,[1] Fabrizio D'Ortenzio,[1] Antoine Poteau,[1] and Alexandre Mignot[1]

Received 21 December 2010; revised 7 March 2011; accepted 28 March 2011; published 28 June 2011.

[1] Eight autonomous profiling floats equipped with miniaturized radiometers and fluorimeters have collected data in Pacific, Atlantic, and Mediterranean offshore zones. They measured in particular 0–400 m vertical profiles of the downward irradiance at three wavelengths (412, 490, and 555 nm) and of the chlorophyll *a* fluorescence. Such autonomous sensors collect radiometric data regardless of sky conditions and collect essentially uncalibrated fluorescence data. Usual processing and calibration techniques are no longer usable in such remote conditions and have to be adapted. The proposition here is an interwoven processing by which missing parts of irradiance profiles (due to intermittent cloud occurrence) are interpolated by accounting for possible changes in optical properties (detected by the fluorescence signal) and by which the attenuation coefficient for downward irradiance, used as proxy for [Chl *a*] (the chlorophyll *a* concentration), allows the fluorescence signal to be calibrated in absolute units (mg m^{-3}). This method is successfully applied to about 600 irradiance and fluorescence profiles. Validation of the results in terms of [Chl *a*] is made by matchup with satellite (MODIS-A) chlorophyll (24.3% RMSE, N = 358). Validation of the method is obtained by applying it on similar field data acquired from ships, which, in addition to irradiance and fluorescence profiles, include the [Chl *a*] HPLC determination, used for final verification.

Citation: Xing, X., A. Morel, H. Claustre, D. Antoine, F. D'Ortenzio, A. Poteau, and A. Mignot (2011), Combined processing and mutual interpretation of radiometry and fluorimetry from autonomous profiling Bio-Argo floats: Chlorophyll *a* retrieval, *J. Geophys. Res.*, *116*, C06020, doi:10.1029/2010JC006899.

1. Introduction

[2] Launched in 1999, the Argo project is a great success in the advancement of Physical Oceanography. With presently an array of about 3000 free-drifting profiling floats, the project delivers in quasi-real time quality-controlled temperature and salinity data for the upper 2000 m of the global ocean.

[3] The miniaturization of optical and bio-optical sensors is such that their implementation on robotic platforms, like profiling floats and gliders, is now possible. Based on the Argo program, the perspective of global-scale monitoring of some biological and optical parameters of the ocean's interior is presently becoming a reality [*Claustre et al.*, 2010; *Johnson et al.*, 2009]. With these emerging tools, a vertical resolution for the bio-optical properties, similar to the resolution typical of the hydrological parameters, is now achievable. Actually, an even better resolution (meter scale) is reachable thanks to iridium telemetry.

[4] New challenges arise from the automated way of observing the bio-optical properties of the ocean. Indeed, conversely to what happens when the same kinds of equipments are operated from a ship, these bio-optical data are collected in environmental conditions which are out of the operator's control. Calibrations/characterizations, as initially provided by manufacturers, are the only piece of information available for the rest of the platform life. Therefore, and under these constraints, new specific data processing and management procedures have to be developed. They are needed for the delivery of quality-controlled data, both in quasi-real time and in delayed mode (in the same manner as the Argo project proceeds for physical parameters). The internal consistency of the final products is a great challenge to fulfill the scientific requirements, in particular to allow the future extraction of climatic trends from such an automated "bio" platforms array. The development of adequate procedures is needed in the early stage of the observing system implementation.

[5] In the present paper, we examine only the way of processing the data of two specific bio-optical sensors: one measures the stimulated fluorescence of chlorophyllous pigments (excitation at 470 nm, emission at 690 nm), while the second one measures the downward irradiance at three

[1]Laboratoire d'Océanographie de Villefranche, UMR 7093, Université Pierre et Marie Curie, CNRS, Villefranche-sur-Mer, France.

0148-0227/11/2010JC006899

wavelengths (λ = 412, 490, and 555 nm). Two kinds of difficulties arise when transforming the raw data into robust geophysical products.

[6] The first and practical problem is related to the large amount of data expected from a long-term deployment of many autonomous profilers. There is no need to elaborate on this aspect; suffice it to say that the answer is in developing, as far as possible, quasi-automatic processing techniques, even if at the end of the process a visual quality control will inevitably be needed. The second difficulty is more fundamental and lies in the use of self-operating sensors that collect data in uncontrolled conditions. The answer to this problem is more complex and depends on the parameters, as examined below.

[7] The transformation of the raw fluorescence signal into a so-called "Chl *a* equivalent concentration," as made through the use of the manufacturer's constant scale factor, provides only a rough indication. Indeed, the in vivo fluorescence signal and its diel variability depend on many factors: first on the taxonomical composition of the local species assemblage and then on the physiological state of this algal community (life cycle, division rate, light regime and history, nutrient availability, etc.) [*Althuis et al.*, 1994; *Babin*, 2008; *Claustre et al.*, 1999; *Cunningham*, 1996; *Falkowski and Kiefer*, 1985; *Kiefer*, 1973a, 1973b; *Marra*, 1997]. Therefore, the calibration of the fluorimeter in terms of realistic chlorophyll *a* concentration, [Chl *a*] remains to be made on a local basis. When such a similar fluorescence sensor is operated from a ship, an associated sampling protocol is (optimally) set up to collect quasi-simultaneously discrete samples, that are thereafter submitted to laboratory analysis (HPLC, for instance). By this way and through appropriate interpolation, each individual fluorescence profile can be, in principle, quantitatively "calibrated." Nothing equivalent can be made when a sensor, embarked on a profiling float, is left alone.

[8] Beside the need for such a local calibration, there are two other flaws affecting the fluorescence data, as illustrated by Figures 1b and 1d. Ostensibly, the nominal "dark count" provided by the manufacturer which is subtracted from the output signal is often insufficient to remove the notable Chl *a* equivalent values still found at depth where the algal biomass is normally vanishingly low (apart perhaps from exceptional conditions of deep convective mixing). The second problem is of photophysiological origin, and lies in the well known occurrence of the daytime nonphotochemical quenching (NPQ) at high irradiance [see, e.g., *Cullen and Lewis*, 1995]. Regardless of the underlying causes (see, e.g., description by *Sackmann et al.* [2008, and references therein]), the net effect of this phenomenon is a decrease of the fluorescence emission (per unit of Chl *a*), when the phytoplanktonic cells are exposed to high, over saturating, solar illumination (an instance is provided by Figure 1d). Such conditions are encountered within the upper layers of the ocean, and for sunny days. In total, converting the signal into a true chlorophyll *a* concentration is not straightforward.

[9] With regard to irradiance (Figure 1a), three kinds of perturbations generally affect the vertical profiles. First, below a certain level of irradiance (about 0.5 μW cm^{-2} nm^{-1}), the signal is drowned inside the dark noise and is no longer useful. According to typical irradiance values at the surface (~10^2 μW cm^{-2} nm^{-1}), the profiles can still reach the 0.5% light level before entering the dark noise background. Second, the verticality of the sensor is adversely affected by the wave's motion near the surface; in addition, these waves induce "lens effects," i.e., a focusing and defocusing of the downward radiant flux [*Zaneveld et al.*, 2001]. These lens effects result in fast fluctuations which propagate downward at depths which depend on (actually increase with) the clarity of the water. Finally, the third source of noise is essential due to intermittent cloud occurrences. The downward irradiance vertical profiles are captured at a predetermined time (generally at local noon), regardless of external conditions (clouds, sky and sea state). During such an autonomous acquisition, passing clouds induce perturbations, easily recognizable for they affect synchronously all spectral channels. In case of thin clouds, the perturbation is less detectable. When similar measurements are performed from a ship, beside the visual control of the sky state and the possibility of selecting the most favorable window for the radiometric measurements, there is normally an above surface reference sensor monitoring the incident irradiation on the deck. Appropriate corrections, allowing the variations in the incident solar flux during the cast to be accounted for, are thus possible. With a float, however, the absence of such an above surface device prevents an autonomous cloud correction from being performed.

[10] The present study attempts to circumvent the various difficulties mentioned above.

2. Materials and Methods

2.1. Instruments and Data

[11] The "PROVBIO" free-drifting profiler is a PROVOR profiler, additionally equipped with autonomous and independent bio-optical sensors, namely, a (Satlantic) OC4 radiometer, a (WET Labs) ECO triplet puck comprising a chlorophyll fluorimeter, a sensor for the CDOM fluorescence and a backscattering detector, and a (WET Labs C-Rover) beam transmissometer. The nominal mission includes acquisition of a CTD profile from the depth corresponding to 1000 m up to the surface, whereas the bio-optical sensors operate from about 400 m up to the surface. The frequency of bio-optical casts can be modified; depending on season and location, upward casts have been programmed every 2, 5, or 10 days. According to the normal protocol, the float emerges from the sea around local noon; thanks to iridium two-way communication, three upward casts have been exceptionally programmed on the morning, noon, and evening of the same day.

[12] Since 2008, eight PROVBIO floats have been deployed and have collected data over a time period of about 2 years (see also Table 1): (1) two floats are in the Mediterranean Sea, with a view of comparing the trophic regimes in the northwestern basin and in the eastern levantine basin (floats denoted MED_NW_B02 and MED_LV_B06, respectively); (2) two floats are in the North Atlantic, namely, in the Irminger Sea (NAT_IS_B01), and in the Iceland Basin (NAT_IB_B03), with the particular aim of studying the progression and fate of the spring phytoplankton bloom; (3) two floats are north of Hawaii (PAC_NO_B05 and PAC_NO_B08), in the eastern sector

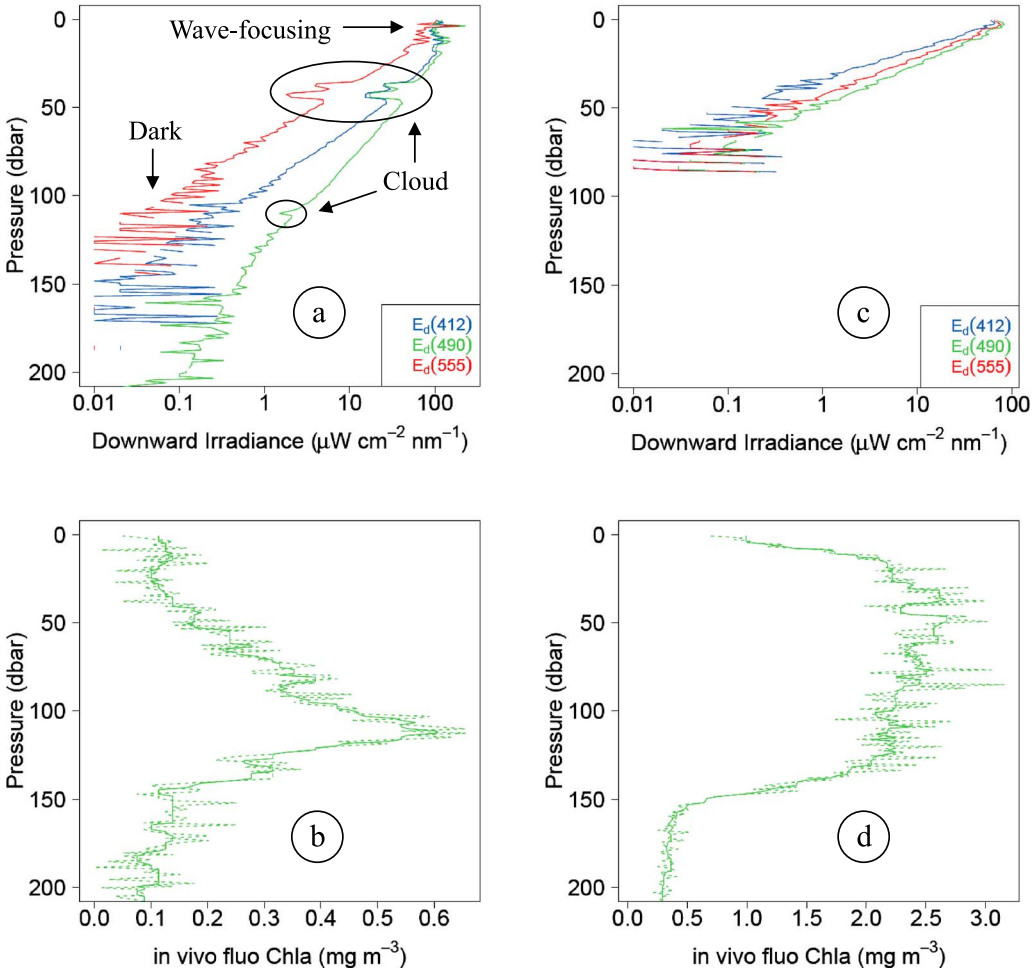

Figure 1. Examples of raw data as recorded by two floats. (a and b) In eastern Mediterranean Sea (32°72′E, 33°75′N; 13 September 2008, 09:51 UT) downward irradiance (units μW cm^{-2} nm^{-1}) at three wavelengths as indicated (Figure 1a) and fluorescence profile processed with the constant parameters (dark count and slope) as provided by the manufacturer (units mg Chl *a* m^{-3}) (Figure 1b); the solid green line shows the result of applying a seven-point median filter on the initial fluorescence profile. A strongly developed deep chlorophyll maximum (DCM) occurs at 110 m. (c and d) Same as Figures 1a and 1b but for a station in the North Atlantic (16°18′W, 60°06′N; 5 May 2009, 13:56 UT). Note that converse to the Mediterranean examples, the irradiance profiles are not cloud contaminated (perhaps affected by mist). The fluorescence profile is depressed near the surface as an effect of nonphotosynthetic quenching and otherwise shows a rather uniform [Chl *a*] distribution within a thick mixed layer (140 m).

of the North Pacific gyre; and (4) two floats are near Easter Island, within the hyperoligotrophic South Pacific gyre (PAC_SO_B04 and PAC_SO_B07).

[13] The database includes the time and geographical (GPS) information, the physical parameters (depth, temperature, and salinity), the bio-optical parameters (namely: the backscattering coefficient at 532 nm, the beam attenuation coefficient at 660 nm, and the fluorescence by colored dissolved organic matter).

[14] Two other kinds of parameters are of particular interest for the present study:

[15] 1. The stimulated fluorescence by chlorophyllous pigments; the raw signals (counts) of the sensor are transformed into "Chl *a* equivalent concentrations," expressed as mg m^{-3}, via the scale factor provided by the manufacturer, and after the nominal instrument-specific dark counts have been subtracted; the scale factor results from a calibration made by using a monoculture of the phytoplankter *Thalassiosira weissflogii*.

[16] 2. The spectral downward irradiances, $E_d(412)$, $E_d(490)$, and $E_d(555)$, expressed as μW cm^{-2} nm^{-1}, according to information provided in the calibration sheet report. The data are averaged before being transmitted in such a way that the achieved vertical resolution is 1 m.

2.2. First Corrections to the Fluorescence Profiles

[17] After the dark count provided by the manufacturer has been subtracted, the fluorescence residual signal detected

Table 1. Relevant Information Concerning the Eight PROVBIO Floats Involved in the Present Study

Float[a]	Start Date	End Date	Number of Profiles at Noon
MED_NW_B02	1 May 2008	14 Mar 2010	140
MED_LV_B06	27 Jun 2008	8 Nov 2009	100
NAT_IB_B03	30 Jun 2008	12 May 2010	120
NAT_IS_B01	1 Jul 2008	17 May 2009	42
PAC_NO_B05	15 Aug 2008	29 Oct 2009	50
PAC_NO_B08	15 Aug 2008	29 Oct 2010[b]	86
PAC_SO_B04	3 Dec 2008	6 Mar 2010	50
PAC_SO_B07	3 Dec 2008	20 Jan 2010	46
Total			634

[a]The trajectories of the floats during their entire life can be seen at http://www.obs-vlfr.fr/OAO.
[b]This float is still working.

at depth is still nonnull and is considered as an instrumental noise (see Appendix A). Indeed, it can be safely assumed that the chlorophyll *a* concentration at depths larger than 300 m is zero, so that the fluorescence profile is simply reset to zero beyond this level; this deep signal is subtracted as an offset along the whole profile. It was expected that this dark noise could be considered as constant and typical of each fluorometer; in reality, it is not exactly the case, so that the correction is to be made profile by profile. The raw data contain spikes and noises which are smoothed by applying a median filter extended over seven consecutive points.

[18] The correction for nonphotochemical quenching is more problematic. A correction may be envisaged in the occurrence of a well-mixed upper layer. In such a case, it can reasonably be assumed that [Chl *a*] is constant within this layer and that the depressed fluorescence signal is only a consequence of quenching when approaching the surface. The density profile is generated from the temperature and salinity profiles, and the depth where a density increment of 0.03 kg m^{-3} (in reference to the density at 10 m) is observed is considered as the basis of the mixed layer. The fluorescence signal around this depth is extrapolated toward the surface. This correction is optional, because the homogeneity within the mixed layer is a plausible presumption, but it is not a certainty. In case of stratified waters, there is no longer a logical basis for such a correction.

[19] After the above corrections are made, a fluorescence profile, denoted fluo(z) where z is depth, is obtained. It is supposed that the true chlorophyll *a* concentration along the vertical, denoted [Chl *a*](z) (units mg m^{-3}), is linearly related to the fluorescence signal, via a proportionality factor F

$$[\text{Chl } a](z) = \text{F fluo}(z) \tag{1}$$

In the following, F will be considered as constant over depth; this simplifying assumption will be discussed later on. The factor F cannot be considered only as a typical feature of the instrument; it must be considered also as a local property. Indeed, the stimulated fluorescence emission per unit of chlorophyll *a* concentration may (and generally does) vary according to composition, physiological state of the algal population, and ambient light [see, e.g., *Fennel and Boss*, 2003]. As previously shown [*Maritorena et al.*, 2000; *Morrison*, 2003], the in situ quantum yield of Sun-induced ("natural") fluorescence is notably varying with algal assemblages, light regime, and depth. If this yield and the present factor F differ, they are certainly not completely disconnected. Therefore, F is to be determined profile per profile. Its assessment is examined below in conjunction with the processing of the irradiance profiles.

2.3. Fluorescence Profiles and Irradiance Profile Connections

[20] By using the definition of the diffuse attenuation for downward irradiance $K_d(\lambda, z)$, the irradiance at the wavelength λ, and a depth Z, $E_d(\lambda, Z)$, can be expressed as a function of the irradiance just below the surface, $E_d(\lambda, 0-)$, according to

$$E_d(\lambda, Z) = E_d(\lambda, 0-) \exp\left(- \int_0^z K_d(\lambda, z) dz \right) \tag{2}$$

where the integral represents the (dimensionless) "optical depth" corresponding to the geometric 0-Z depth interval, and where $K_d(\lambda, z)$ is allowed to vary with depth. The irradiance profiles are obtained as a series of discrete data with a vertical resolution Δz of about 1 m; the above relationship can thus be written

$$\ln E_d(\lambda, Z) = \ln E_d(\lambda, 0-) - \sum_1^n K_d(\lambda, z) \Delta z \tag{3}$$

where the summation extends over the n layers of thickness Δz, between 0 and Z.

[21] This equation is an analytical formulation of the actual in situ irradiance profiles (see, e.g., Figures 1a and 1b), and their comparison suggests two remarks: (1) in the portions where the profile is "clean" (no cloud perturbation), K_d is well defined and the above expression accounts for the entire profile; conversely, in case of cloud shadowing (e.g., some portions in Figure 1a), equation (3) becomes inappropriate, and (2) because of the recurrent near-surface noise, the initial $E_d(0-)$ value is experimentally ill determined, but it is derivable from equation (3) if the upper part of the profile is cloud free.

[22] The proposition at this stage is to try to find out a help for restoring the entire irradiance profile by using the fluorescence profile. Fluorescence can detect a change in chlorophyll *a* concentration, which impacts the optical properties, and thus the attenuation coefficient K_d (and hence the irradiance profile). Reciprocally, K_d, seen as a proxy of [Chl *a*], can help in calibrating the fluorescence data (in finding F, equation (1)). The rationale is thus to take advantage of this link that exists, at least in case 1 waters, between the attenuation coefficient K_d and [Chl *a*] [*Morel*, 1988; *Morel and Maritorena*, 2001]. By approximation, K_d can be seen as the sum of two terms

$$K_d(\lambda) = K_w(\lambda) + K_{bio}(\lambda) \tag{4a}$$

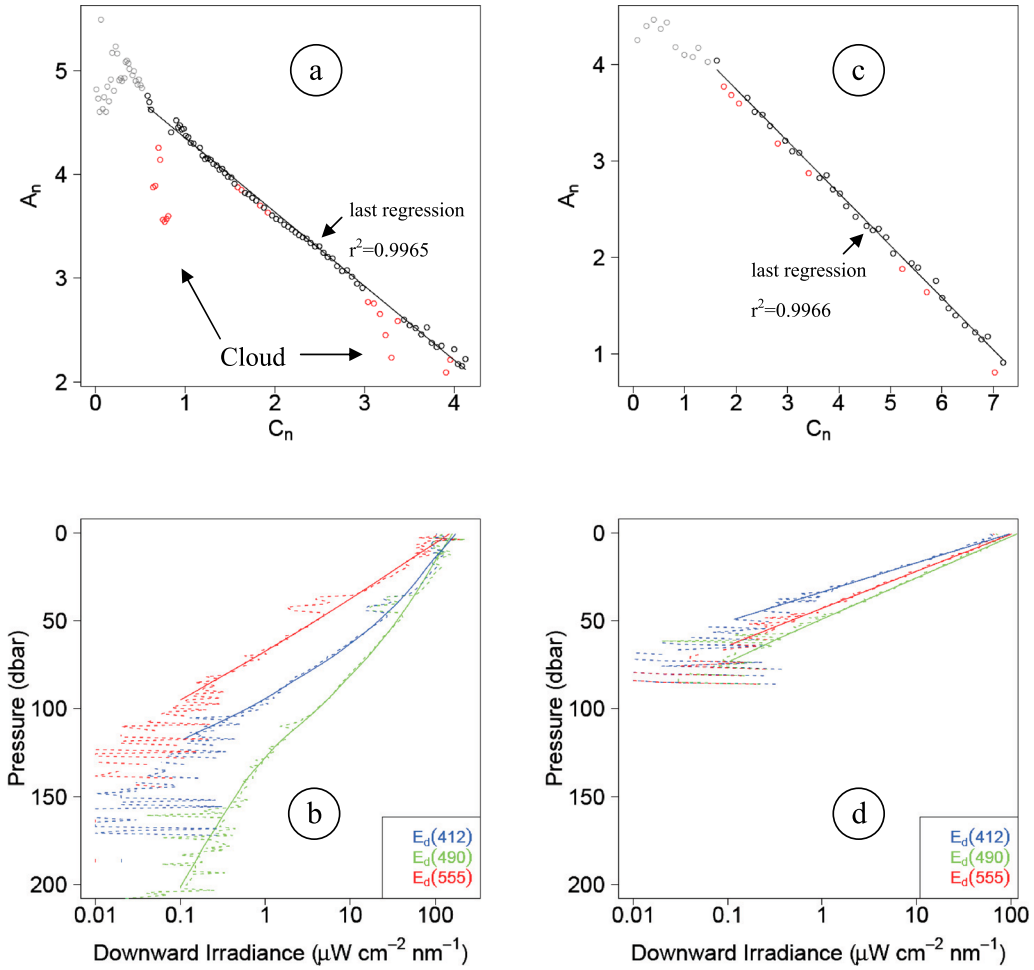

Figure 2. (a and b) The Mediterranean cast as in Figures 1a and 1b. (c and d) The North Atlantic cast, as in Figures 1c and 1d. Figures 2a and 2c show graphically the application of equations (6a) and (6b) when the number (n) of elementary layers is increasing. Figures 2b and 2d show the restored irradiance profiles (heavy lines) for the same stations, superimposed on the initial profiles (dashed lines, from corresponding Figure 1).

where $K_w(\lambda)$ represents that part of attenuation due to the (pure) seawater, which is a constant for a given wavelength, and K_{bio}, represents the other part of attenuation, which results from the presence of biological material (phytoplankton plus accompanying particulate and dissolved substances). Regression analyses (between the log-transformed of the quantities K_{bio} at each wavelength, and [Chl *a*]) showed that $K_{bio}(\lambda)$ varies as a nonlinear function of the [Chl *a*], according to [*Morel*, 1988; *Morel and Maritorena*, 2001]

$$K_d(\lambda) = K_w(\lambda) + \chi(\lambda)[\text{Chl } a]^{e(\lambda)} \tag{4b}$$

and these analyses provided the coefficients $\chi(\lambda)$ and exponents $e(\lambda)$.

[23] By introducing equation (4b) into equation (3), and considering that [Chl *a*] varies with depth, it becomes

$$\ln E_d(\lambda, z) = \ln E_d(\lambda, 0-) - \sum_1^n \left[K_w(\lambda) + \chi(\lambda)[\text{Chl } a, z]^{e(\lambda)}\right]\Delta z \tag{5}$$

[Chl *a*] is still unknown at this stage, as the factor F in equation (1) has not been determined. By using fluo as a surrogate for [Chl *a*], and reassembling equations (1) and (5), the final expression is

$$\ln E_d(\lambda, z) + \sum_1^n K_w(\lambda)\Delta z = \ln E_d(\lambda, 0-) - F^{e(\lambda)} \sum_1^n \left[\chi(\lambda)\text{fluo}(z)^{e(\lambda)}\right]\Delta z \tag{6a}$$

The mutual help expected from the simultaneous consideration of the two quantities, irradiance and fluorescence is not self-evident, since an additional unknown (F) has been introduced. The solution of the system cannot be analytical, but is conceivably reachable through an iterative process. Equation (6a) can be represented under the simple form

$$A_n = B_0 - S\ C_n \tag{6b}$$

A series of n similar equations is obtained by incrementing the order n, and so by increasing the thickness of the layer under consideration. All these relationships are linear and contain the same unknown $S = F^{e(\lambda)}$. Each of them contains a known term, A_n, which is computed from the successive

$E_d(z)$ data, and from K_w; this term decreases when z (i.e., when n) increases. All these relationships also contain the same constant term, (experimentally) undetermined, namely, $B_0 = \ln E_d(\lambda, 0-)$.

[24] The coefficient C_n, computed from the fluo data, represents (in relative units) an optical thickness; C_n increases with n, i.e., the number of elementary layers considered.

2.4. Combined Processing Involving Both Downward Irradiance and Chl Fluorescence

[25] First, the deep noisy irradiance values, as well as the noisy near-surface values are automatically removed to keep a "clean" $E_d(z)$ profile. The upper part of the profiles is automatically discarded down to an optical depth equal to 0.69 (a depth where $E_d(z)$ is reduced to 50% of its value at the surface). The clean profiles nevertheless may include some portions affected by clouds and not yet identified as such. By increasing n step by step and using equation (6), a series of successive A_n and corresponding C_n values are generated, and A_n can be plotted versus C_n (examples in Figures 2a and 2b). While C_n monotonously increases with increasing n, A_n decreases; this decrease is regular if the E_d profile is featureless (noise free), or is irregular if $E_d(z)$ is affected, i.e., depressed by clouds (see Figure 2a).

[26] A first linear regression analysis is performed at this stage between the quantities A_n and C_n. The unknown S is now the slope of the regression line and the intercept at $n = 0$ ($C_n = 0$) provides the B_0 value, i.e., $\ln E_d(\lambda, 0-)$. This is the simple situation when there is no cloud (almost the case in Figure 2c), but this procedure is intended for identifying and then restoring the portion of the profile which is contaminated by clouds. When the first regression analysis is performed as described above, the clouds show themselves as depressed A_n values (red dots in Figure 2a). At this stage, an automatic procedure eliminates all the points below the first computed regression line. A second regression analysis is then performed with the remaining points; this process of regression, followed by an elimination of the outliers under the regression line, is repeated until a criterion based on the residual (actual $A_n > 98\%$ of the value predicted by the regression line) is satisfied; actually, two, scarcely three, iterations/eliminations are sufficient. The last regression straight line is adopted as representing the undisturbed relationship, namely, the relationship which would have been observed in absence of clouds (and of some noise near the surface, when insufficiently eliminated).

[27] Several quantities are now determined.

[28] 1. The intercept (at $n = z = 0$) is B_0, and thus provides the $E_d(\lambda, 0-)$ value.

[29] 2. The slope of the regression line, S, provides the factor F needed for the calibration of the fluorimeter, according to

$$F = S^{1/e(\lambda)} \tag{7}$$

[30] 3. The contaminated portions of the $E_d(\lambda, z)$ profile can be restored by using again equations (6a) and (6b); equations (6a) and (6b) are now operated as a prognostic tool, since all terms in the right-hand side of the equation have been determined, so that A_n, and therefore $E_d(\lambda, z)$, can be computed in those portions where they were lacking, whereas the other portions remain essentially unchanged. It is worth noting that the above method simply ensures a continuity in the interpolation process restoring the $E_d(\lambda, z)$ profile. Importantly, this method is able to account for a change in the chlorophyll *a* concentration that influences the distance between the successive C_n values, and thus the curvature of the E_d profile; such a curvature remains undetected if localized in a portion of the profile obscured by clouds. The absolute E_d values outside of the disturbed portions of the profile are not altered by this process. With the factor F now determined through equations (6a) and (7), [Chl *a*] can be determined in absolute units (equation (1)).

[31] 4. The above described process obviously fails when too many clouds occur during the irradiance cast. In such a case the last regression line is not significant (the criterion for rejection is $r^2 < 0.98$), or its significance is restrained to small portions of the depth interval, so that the E_d profile cannot be properly reconstructed.

[32] 5. Note that the problem of clouds and light fluctuations has been circumvented in another way by *Nahorniak et al.* [2001] and *Brown et al.* [2004]. Under the assumption made by Nahorniak et al. and Brown et al. of an unchanged spectral composition of incident radiation, whatever the cloudiness, the ratio of spectral irradiance at two wavelengths (and at a given depth) remains unchanged, and thus the difference in the corresponding attenuation coefficients would be insensitive to the occurrence of clouds. This assumption, adopted for multispectral analysis does not allow the attenuation coefficient at a single wavelength, as needed in the present study (see below), to be derived during the transient regimes imposed by passing clouds.

2.5. Spectral Dependency

[33] The downward irradiance measurements are performed at 412, 490, and 555 nm. At least in principle, the process above described which combines irradiance and fluorescence measurements can be applied at any wavelength. For the wavelengths available, the empirical equation (4b) takes the following values (see "LOV data" for case 1 waters of *Morel et al.* [2007b]):

$$K_d(412) = 0.00793 + 0.1333[\text{Chl } a]^{0.6199} \tag{8a}$$

$$K_d(490) = 0.01660 + 0.0825[\text{Chl } a]^{0.6529} \tag{8b}$$

$$K_d(555) = 0.06053 + 0.0561[\text{Chl } a]^{0.5070} \tag{8c}$$

These numerical values indicate that the relative influences of the two components (pure water and biological material) in forming the attenuation coefficient markedly differ according to the wavelength; for instance, the influence of pure water is almost 8 times higher at 555 than at 412 nm, whereas the influence of Chl *a* is approximately halved from 412 to 555 nm. As a practical consequence, K_d at 555 nm is weakly sensitive to [Chl *a*], so that it is not useful in the process (based on equation (6a)) which leads to the S and F estimates. In contrast, K_d at 412 or 490 nm can be used. The F factor, in principle, is totally independent of the wavelength considered for its derivation, and must stay

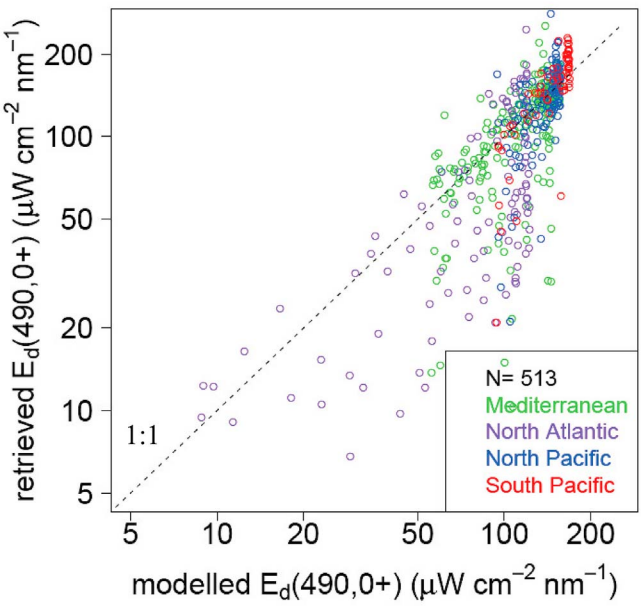

Figure 3. Retrieved downward irradiances just above the surface (from the B_0 term in equation (6b)) compared with the values computed according to *Gregg and Carder* [1990] for the location, day and time corresponding to the end of the upward casts. Note that the low values are for casts occurring in the morning or evening (North and South Pacific).

unchanged whether 412 or 490 nm are used when operating equation (6a) and (7). Such a statement, however, would imply that equations (8a) and (8b) are strictly exact and fully compatible; rigorously, it is never the case. As being statistical products, these expressions are representative of an average bio-optical situation, so that statistical fluctuations around the mean trends and between their spectral expressions are to be expected [*Morel and Maritorena*, 2001; see also *Ciotti et al.*, 1999]. Actually, systematic deviations, affecting $K_d(412)$, have already been detected in some specific environments [*Morel et al.*, 2007a] and discussed in section 3.3.

3. Results and First Discussion

[34] The total number of profiles (for irradiance and fluorescence) collected near noon by the eight floats amounts to 634 (Table 1), among which 508 can be successfully processed. The processing cannot be completed in case of sensor failure or when the cloud cover is too much unstable. Profiles occasionally obtained close to sunset and sunrise for other (and specific) purposes are discarded.

3.1. Irradiance Profiles

[35] Together with the regression significance (r^2), the visual inspection of the initial raw irradiance profile, and then of the intermediate steps in the processing (compare Figure 2) are subjective ways of assessing the quality of the restored profile. More appropriate tools for an automatic treatment are nonetheless needed.

[36] A first possible verification consists in examining if the irradiance values, when extrapolated above the surface, $E_d(0+)$, are plausible when accounting for the date, time and geographical location. The second verification deals with the $K_{bio}(\lambda)$ values that derive from the irradiance profiles; the test examines the validity and compatibility of the retrieved values.

[37] The extrapolated $E_d(0+)$ values can be compared to the theoretical values computed for a cloudless standard maritime atmosphere. The model proposed by *Gregg and Carder* [1990] is used for that purpose. The extrapolated values assume that there is no cloud obscuring the solar disk, even if the entire sky is not necessarily cloud free when the float reaches the ocean surface. Reflecting clouds approaching the sun's disk may slightly and briefly enhance the irradiance above the value for cloud free sky (it is an infrequent situation), while semitransparent clouds and haze depress the above surface irradiance (a more common situation). The comparison between the extrapolated and the modeled $E_d(0+)$ values is illustrated by Figure 3. The scatter is a rather high ($r^2 = 0.68$, N = 513). The distribution of the points, with extrapolated $E_d(0+)$ values often below the modeled $E_d(0+)$ values, suggests that overcast or misty conditions are frequent; the unexpected presence of rather numerous points above the 1:1 line suggests that the inaccuracies in the extrapolation process are the main cause of such deviations, rather than exceptional reflecting clouds.

[38] After the irradiance profiles (at 412 and 490 nm) have been cleaned and their missing segments restored, the downward irradiance attenuation coefficients can be computed, and from them, the partial coefficients $K_{bio}(412)$ and $K_{bio}(490)$ are derived. Note that this derivation is only possible for intermediate depths, since the noisy upper part of the profile has been discarded. These K_{bio} coefficients are plotted on Figure 4, which demonstrates the compatibility of their covariations over 2 orders of magnitude. The dashed line represents the ratio of the χ coefficients in equations (8a) and (8b), equal to 1.62 (the exponents appearing in these equations are close, so that their effect on the ratio can be safely neglected). Note that the $K_{bio}(412)$ values are often above the 1.62:1 line which reflects a higher relative yellow substance content at intermediate depths (compared to the content in upper layer where the expression (8a) and (8b) have been obtained). This is particularly true for the Mediterranean waters where the $K_{bio}(412)/K_{bio}(490)$ ratios are systematically higher than the average. This is not surprising according to the particular bio-optical properties and relatively enhanced yellow substance content already observed in this Sea [*Morel et al.*, 2007a; *Morel and Gentili*, 2009].

3.2. Calibration of the Fluorescence Profiles

[39] After the irradiance profiles have been consolidated, the fluorescence profiles can be locally calibrated to retrieve the chlorophyll *a* concentration via the factor F (equations (6a), (6b) and (7)). The factor presently used is obtained via the regression process at the wavelength 490 nm (it is denoted F_{490} when needed). Generally, this factor is below 1 (Table 2), which means that the local algal populations generally fluoresce less per unit of chlorophyll than the phytoplankter cultivated and used by the manufacturer to perform the initial calibration. The temporal fluctuations in the F factor (instances in Figure 5), likely reflect (at least partly) the uncertainties in its derivation;

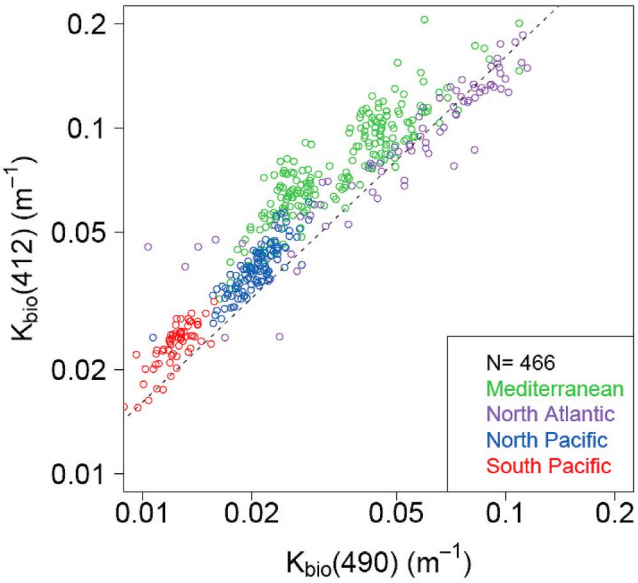

Figure 4. The quantities K_{bio} (see text and equation (4)) derived from the irradiance profiles after they have been restored (compare Figures 2c and 2d); K_{bio} at 412 nm is plotted versus K_{bio} at 490 nm; the dashed line represents the ratio of equations (4a) and (4b) (= 1.62) which assumes that the dependence of this ratio with respect to [Chl *a*] is negligible (the exponents are practically equal).

more probably, they are a response to changing taxonomical and physiological status within the algal populations [see, e.g., *Fennel and Boss*, 2003; *Proctor and Roesler*, 2010].

3.3. Alternative Fluorescence Calibration via F_{412}

[40] As already said, the fluorescence calibration method is in principle totally independent from the wavelength of the irradiance profile used for its derivation. In practice, the $K_d(\lambda)$ which are used as proxies for [Chl *a*], are not equally accurate in representing this pigment concentration, and thus not equally efficient for ensuring the calibration skill. At the wavelength 555 nm, for instance, the diffuse attenuation coefficient is weakly sensitive to the chlorophyll content, so that it is definitely not favorable for a calibration. The wavelength 443 nm, not available with the present floats, would be as efficient as (perhaps more efficient than) 490 nm. The wavelength 412 nm, with $K_d(412)$ also tightly linked to [Chl *a*] (equation (8a)) is an alternative possibility; yet, $K_d(412)$ is also sensitive to the presence of dissolved yellow substance (YS, including nonalgal detrital material), and the sensitivity of K_d to YS is considerably higher at 412 nm than at 490 nm as a result of the increasing absorption of this substance toward the violet end of the spectrum. The additional and variable influence of YS induces deviations in equation (8a). A clear example of such deviations is found by comparing the $K_d(\lambda)$ values in the South Pacific and in the Mediterranean waters [*Morel et al.*, 2007a] (see also Figure 4). To the extent that the relative proportions of the [Chl *a*] and YS are not constant, and are a priori unknown, equation (8a) may be locally inappropriate (equation (8b) is less sensitive). As a conclusion, the use of $K_{bio}(412)$ as a surrogate for [Chl *a*] and for the Chl a fluorescence calibration is uselessly risky; conversely this coefficient would be better adapted for the evaluation of the role of the yellow substance (CDOM).

4. Validations

[41] A validation with regard to the chlorophyll retrieval of the results obtained through the use of the present method when applied to the data of the various floats, as well as a more general validation of the method itself is possible. Such validations require that external, independent, information is available.

4.1. Comparison With MODIS Data

[42] The chlorophyll *a* concentration is a product derived at global scale from space via ocean color radiometry. Specifically, the data of the (NASA) MODIS-A sensor are presently used for the validation, and the [Chl *a*] values produced through the OC3M algorithm [*O'Reilly et al.*, 2000] are compared to those derived from the float data. The 8 day level 3 composites are used to provide possible match up. If there are enough (i.e., at least 3–4) clear sky pixels inside a 0.2° × 0.2° box centered on the float location, the match up with the mean [Chl *a*] value in the box is considered as valid. With such a rather wide temporal and spatial window, there are a considerable number of coincidences available; they are pooled together on Figure 6 and separately shown for each float in Figure 7.

[43] The agreement between the two kinds of [Chl *a*] values is rather good (24.3% RMSE, N = 358), particularly when considering that [Chl *a*] encompass 2 orders of

Table 2. Data Sets Used for the Validation of the Method

Station/Cruise	Date	F_{490}[a]	F_{412}[a]
	BIOSOPE Data Set[b]		
MAR1	26 Oct 2004	0.718	0.592
HNL1	31 Oct 2004	0.575	0.501
STB5	7 Nov 2004	0.693	0.792
GYR2	12 Nov 2004	1.358	1.233
GYR3	13 Nov 2004	1.154	1.263
GYR4	14 Nov 2004	1.186	1.386
EGY2	26 Nov 2004	0.854	0.733
EGY4	28 Nov 2004	0.902	0.778
EGY5	29 Nov 2004	0.811	0.718
UPW1	6 Dec 2004	1.865	1.988
UPX2	10 Dec 2004	2.198	2.495
	BOUSSOLE Data Set[c]		
62	16 Mar 2007	2.144	1.769
63	16 Apr 2007	2.447	3.187
65	21 Jun 2007	2.206	NA
66	23 Jul 2007	3.720	2.918
67	4 Sep 2007	2.034	4.028
68	7 Oct 2007	2.955	4.462
69	10 Nov 2007	3.699	5.795

[a]The factors for the fluorescence calibration, F_{490} and F_{412}, obtained when using the irradiance profiles at the wavelengths 490 nm and 412 nm, respectively. NA, not available.
[b]The locations of the stations along the BIOSOPE transect are given by *Claustre et al.* [2008].
[c]The "Boussole" site [*Antoine et al.*, 2008] is regularly visited (cruise number indicated).

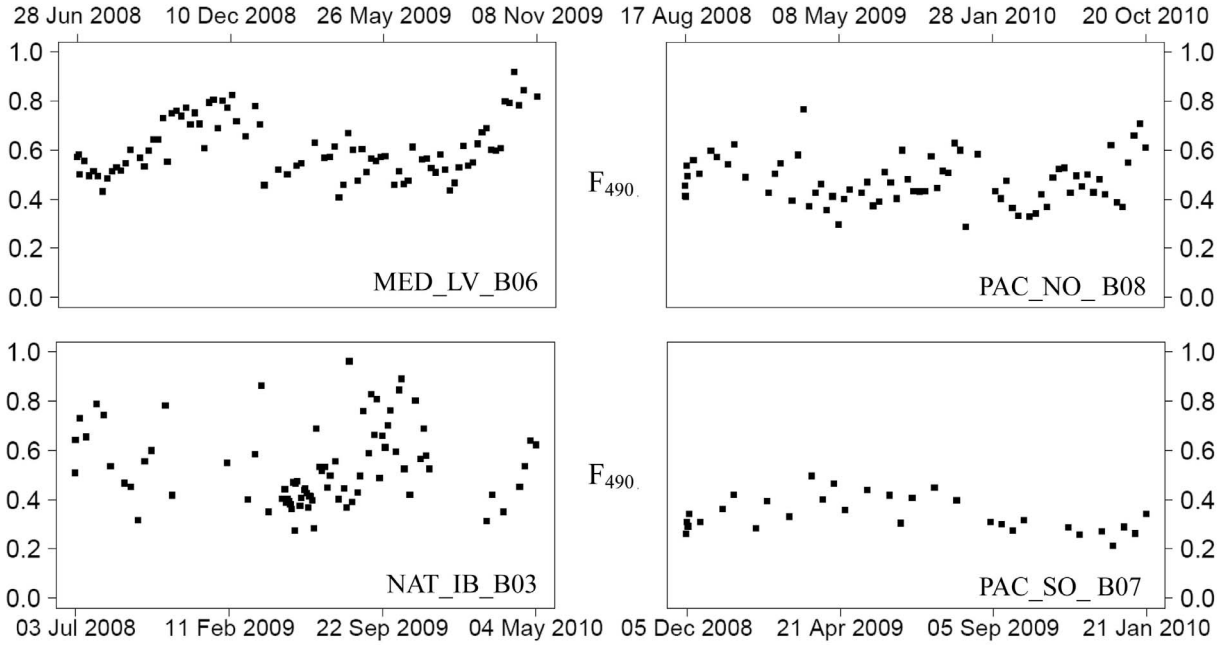

Figure 5. Examples of time series of the calibration fluorescence factor, F_{490}, obtained from successive casts by four floats in various environments.

magnitude (Figure 6) and that both kinds of determinations have their own uncertainty. For the values derived through the empirical algorithm such as OC3M, it is commonly admitted that the uncertainty is about ±30% [*O'Reilly et al.*, 1998]; for the values derived from the near-surface fluorescence, the uncertainty is not easily quantifiable because the fluorescence responses are variously affected by taxonomic composition, quenching process and irradiance levels [see, e.g., *Cullen and Lewis*, 1995]. The time series in Figure 7, however, demonstrate for many points a very good agreement in the Mediterranean Sea; note that in this Sea the fluorescence data, often affected by the NPQ effect have been corrected for when the mixed layer was well identified (28% of the profiles are corrected in the Western basin and 13% in the Eastern basin). Almost all data in the North Atlantic (90%) were corrected for the NPQ effect. The number of match ups remains low in this zone as cloudy conditions prevail. In terms of number of match ups, the situation is much better in the north Pacific; there, the satellite returns are frequently above those of the floats (the NPQ correction can be emulated only in less than 10% of the cases). Nonetheless, the relative [Chl *a*] variations, as detected by fluorescence or from space, are remarkably coinciding in this zone. In the Southern Pacific gyre, where the lowest [Chl *a*] values occur, the agreement is rather poor (for the float B07), and more satisfying (for B04) but restricted to only few points.

4.2. Validation of the Method

[44] The efficiency of the method can be tested against traditional measurements, performed from a ship in totally controlled conditions and including the [Chl *a*] determinations to be used as "sea truth." The validation will consist of applying to the irradiance and fluorescence field data, similar to those collected by the floats and with similar sensors, the whole processing method in a "blind" manner; in a second step, the fluorescence profiles, recalibrated by using the locally derived F factor, are compared with the HPLC TChl *a* determinations [*Ras et al.*, 2008]; TChl *a* is the sum of the monovinyl and divinyl Chl *a*, including allomers, epimers, and cholophyllide.

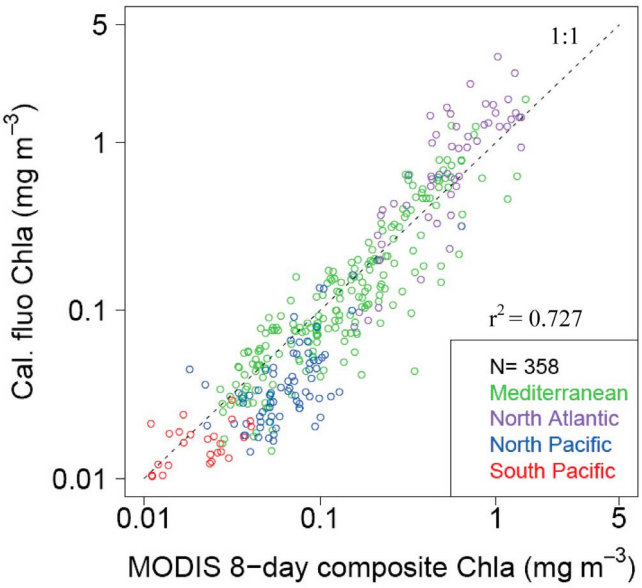

Figure 6. Near-surface [Chl *a*] derived from the fluorescence measurements performed by the eight floats plotted versus the [Chl *a*] values, approximately at the same location and dates, and derived from the MODIS-A radiometric data (see text).

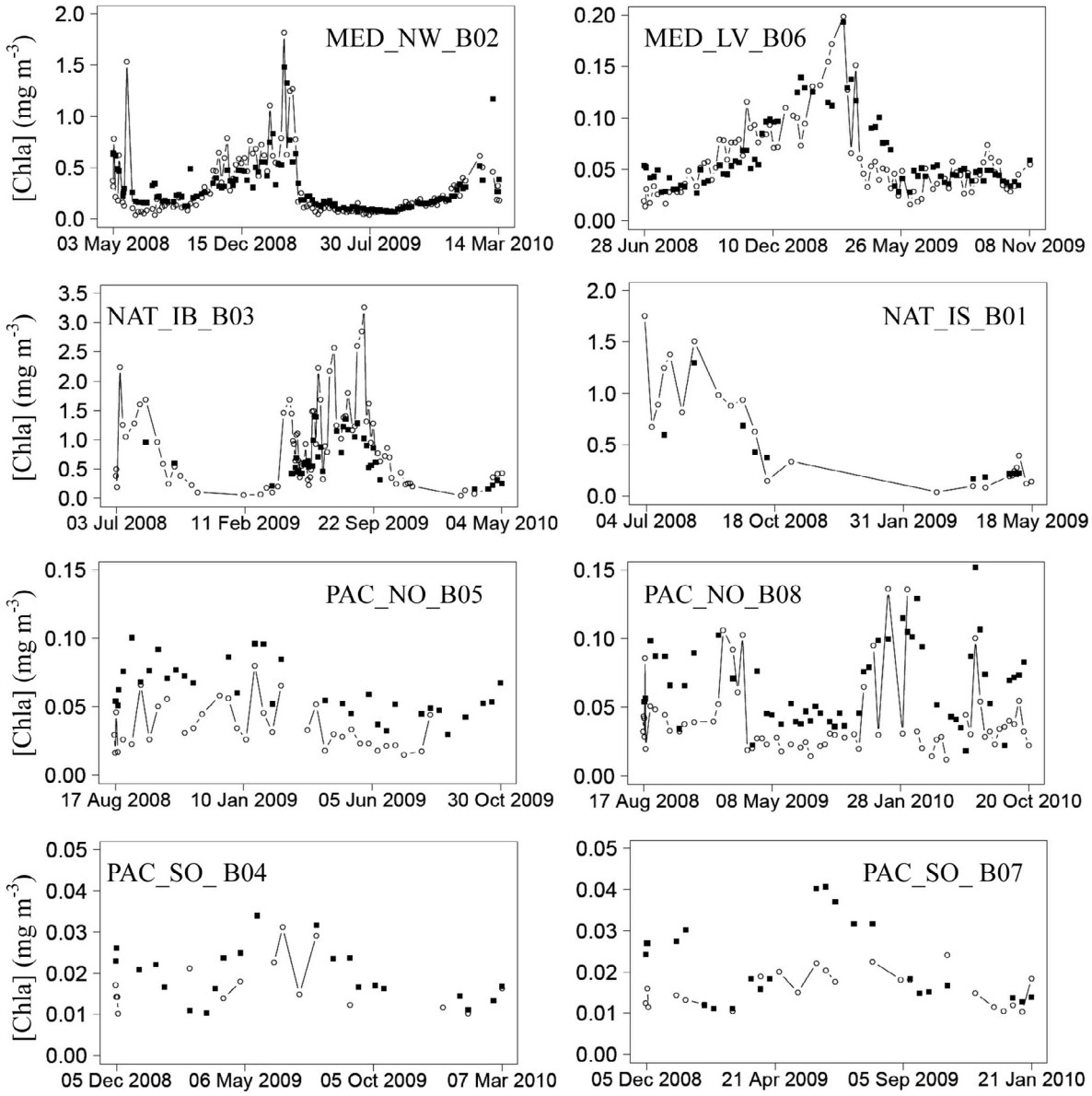

Figure 7. As in Figure 6, but for the eight individual floats; in these time series, the MODIS [Chl *a*] data are represented by square points, the fluorescence-derived [Chl *a*] values are as open circles. Note the large differences in the [Chl *a*] scales and content, according to the location.

[45] The Biosope cruise [*Claustre et al.*, 2008] in the South East Pacific provides all the needed information (irradiances profiles, fluorescence profiles and HPLC data) to proceed to a full validation. The monthly cruises to the "Boussole" site [*Antoine et al.*, 2008] in the northwest Mediterranean Sea provide the same complete set of information. The fluorimeters used during both field experiments are Chelsea instruments (Mk III Aquatracka). As for the WET Labs instruments, the readings of the Chelsea instruments are transformed into fluo(z) profiles via the scale factor provided by the manufacturer; the calibration is made using pure Chl *a* dissolved in acetone, which actually produces a purely arbitrary scale (despite the use of the Chl pigment molecule); the usefulness of such a calibration is to ensure a coherency between the various sensors, or between the various measurements obtained from the same sensor. The local recalibration of these fluo(*z*) profiles via the F factor is made as for the floats measurements. The values of the F factor are given in Table 2 (actually both F_{412} and F_{490} are provided for comparison), and examples of the recalibrated profiles using F_{490} are displayed on Figure 8, together with the HPLC determinations.

[46] The F_{490} factors for these Chelsea instruments are higher than those found for the WET Labs instruments mounted on the floats; these differences originating from the differing calibration techniques have no particular meaning. For the BIOSOPE cruise, F varies considerably with stations, and reaches its highest value in the Peruvian upwelling zone. At the Boussole site, F_{490} is high (~2–3) and only slightly variable (see Table 2).

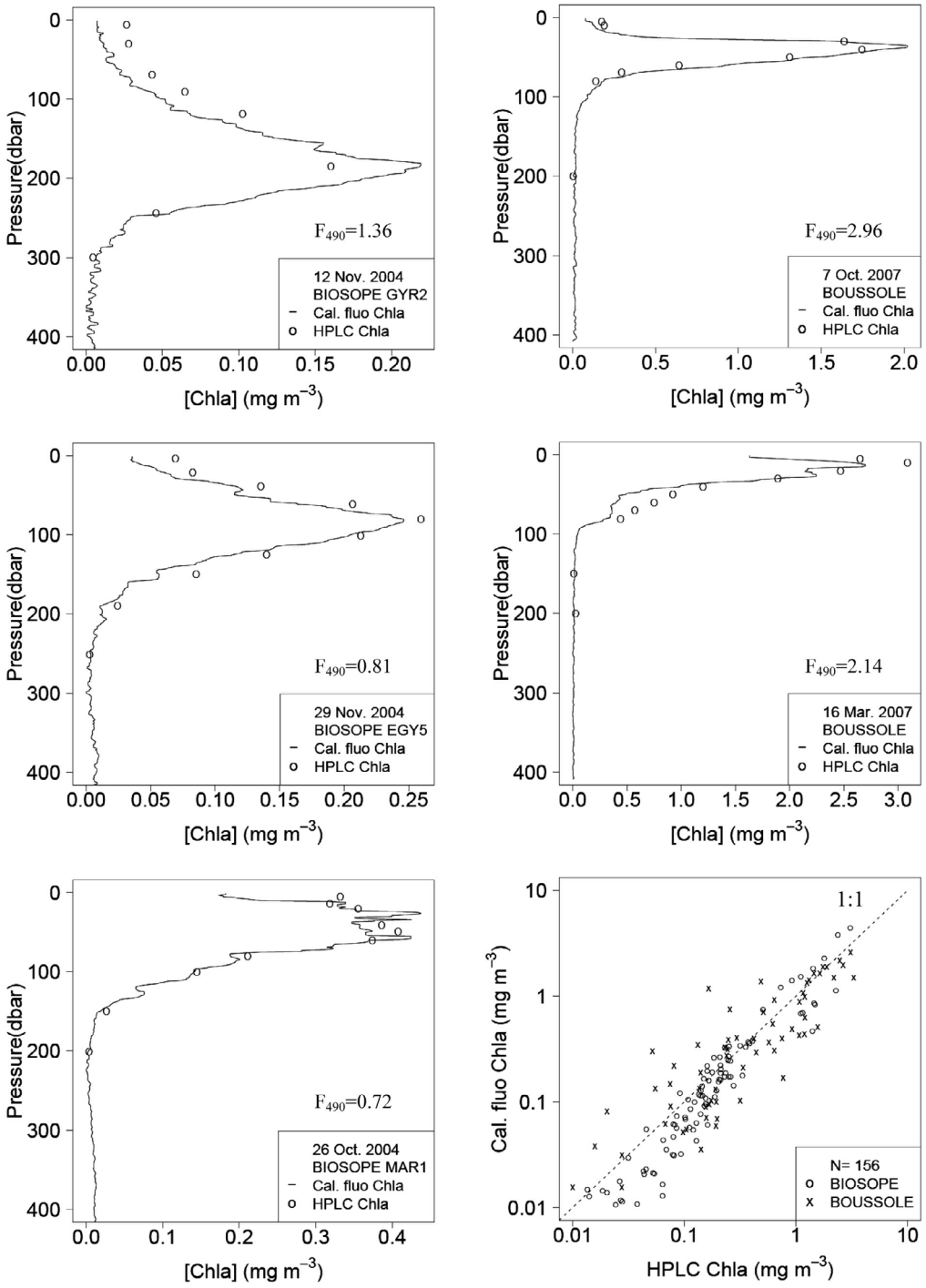

Figure 8. Examples of fluorescence profiles after recalibration in terms of [Chl *a*], compared to HPLC determinations performed on discrete samples at the same location. Bottom right: summary plot showing all available (156) coincident fluorescence and HPLC data; the dashed line is the 1:1 line.

[47] The recalibrated fluorescence profiles making use of these local F_{490} values are in excellent agreement with the HPLC determinations at discrete depths (Figure 8). The examples displayed encompass a variety of trophic situations, relatively to the algal biomass, and to the position of the deep chlorophyll maximum (DCM). A hyperoligotrophic system, represented by GYR2 (BIOSOPE cruise), is characterized by a [Chl *a*] level < 0.05 mg m^{-3} near the surface and a DCM peaking at ~190 m; a mesotrophic system is found near the Marquesas Islands (MAR1). In contrast, eutrophic conditions prevail during the spring bloom in the NW Mediterranean Sea (March 2007). All situations (18 stations in total) including 156 HPLC-fluorescence pairs are shown Figure 8 (bottom right). Figure 8 (bottom right) shows a very good agreement between the fluorescence derived [Chl *a*] and the chemical determinations, over a [Chl *a*]

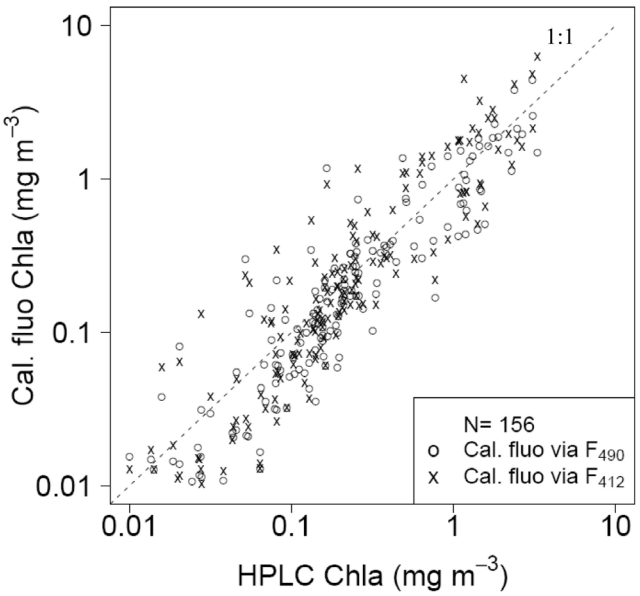

Figure 9. As in Figure 8 (bottom right), recalibrated fluorescence [Chl *a*] is plotted versus the HPLC determinations; the recalibration is made by using either F_{490} or F_{412}; in the first case, $r^2 = 0.76$, and in the second case, $r^2 = 0.69$.

range exceeding 2 orders of magnitude, without significant bias and with a coefficient of determination $r^2 = 0.76$. It can be concluded that the validation of the method is achieved.

[48] If the calibration of the fluorescence profiles is made at the wavelength 412 nm and by using the F_{412} factor instead of the F_{490} factor, the agreement with the HPLC determinations is not dramatically degraded, since the r^2 coefficient decreases only from 0.76 to 0.69 (Figure 9). Nevertheless, it is believed that the wavelength 490 nm, less sensitive to yellow substance fluctuations, is definitely safer for estimating the F factor and the fluorescence calibration.

5. Final Remarks and Conclusions

[49] Several points raised during the presentation of the result were left for further discussions. They are now examined.

[50] About the fluorescence calibration factor, the method based on the slope of the regression (equations (6) and (7)) provides a single value for F (at a given wavelength). In essence, such a single value implies that there would be a unique relationship between the absorptive capacity of the suspended materials (among which phytoplankton are the major absorber at blue wavelengths) and the capacity of reemitting photons through the chlorophyll fluorescence process. Actually, this process, which depends to the first order on the chlorophyll *a* concentration, is also dependent on the taxonomy and the photophysiology of the phytoplanktonic population. Therefore, it is probable that the fluorescence yield (per unit of [Chl *a*]) varies with depth and with the layering of various algal populations, for instance within the DCM where a change in the dominant species may occur. As a consequence, F should not be rigorously constant along with depth. This weakness apparently has a reduced impact, however, as demonstrated by Figure 8. In Figure 8, indeed, varied algal profiles, some with prominent DCM, are nevertheless successfully quantified in terms of [Chl *a*], despite the application of a unique F factor along the vertical.

[51] The varying fluorescence yield mentioned above does not refer to another phenomenon, namely, the nonphotochemical quenching. As already mentioned, NPQ affects the fluorescence response of the algal population inhabiting the upper layers. The solution which is (optionally) adopted here is questionable for two main reasons; first, it cannot be ascertained that the [Chl *a*] profile is strictly uniform within the mixed layer even if this layer can be clearly identified; second, the hypothesis of uniformity cannot be made when the upper layer is a little bit stratified, so that in such a case, there is no sound basis for assuming that the photoinhibition is the sole cause of the fluorescence decrease toward the surface. To get rid of the NPQ ambiguity, the obvious way is to operate nighttime, which is not compatible with a capture of irradiance profiles allowing the fluorescence calibration; so, modified protocols are likely needed.

[52] In addition of being a test for coherency, the comparison of the attenuation coefficients, K(490) and K(412) (compare Figure 4), may provide information about the yellow substance (YS) content and its relative variations. The first determinant of the K coefficients is the absorption coefficient, as shown by the relationship established by *Gordon* [1989]:

$$K \approx 1.04\ \mu_d^{-1}\ a(1 + b_b/a) \tag{9}$$

Here μ_d is the average cosine for downward irradiance, and b_b, is the backscattering coefficient, rather small compared to *a*. Because of the typical ascending slope of the YS absorption toward the shorter wavelengths, the presence of varying amount of this substance has more impact at 412 than at 490 nm on the absorption coefficient, and thus on the K coefficients. It is thus possible to relate such a differential absorption to variations in YS. This potential application is out of the scope of the present paper, however.

[53] The validation of the present method based on field data (including HPLC determinations) has also shown that fluorescence profiles can be successfully (re)calibrated with the help of irradiance profiles. This result is of general application and can be useful for another purpose; indeed, it offers the possibility of improving the manufacturer's initial calibration of any fluorescence sensor. The proxy used for the chlorophyll content, namely, $K_{bio}(\lambda)$, is undoubtedly more representative of the local phytoplanktonic population than the monospecific cultures used for the sensor calibration by the manufacturers (without speaking of the acetone Chl *a* solution). Nevertheless, with the present method, the accuracy of the Chl retrieval will stay limited by the variability in the empirical relationships expressed by equation (8b). The magnitude of the F_{490} factor (Table 2) shows that the recalibration leads to a profound modification of the fluo(z) initial information. Such a recalibration is particularly important in view of the validation of satellite borne ocean color sensors.

[54] In conclusion, it cannot be claimed that the method, as developed and proposed here, is a perfectly rigorous

solution; it is an operational tool, which has been satisfactorily validated. Other kinds of information are also available with the floats as they are presently equipped, such as the backscattering coefficient or the beam attenuation coefficient. These parameters can help in the specification of the mixed layer thickness, for instance [*Sackmann et al.*, 2008]. They, however, cannot bring decisive advantages in the specific issues of cleaning the irradiance profiles or quantifying the fluorescence data; indeed, the relationships between these inherent optical properties and the chlorophyll *a* concentration, or the diffuse attenuation coefficient, are not better than those already represented by equations (8a)–(8c). If the improvements to be expected from their use cannot be considerable, these coefficients can provide useful confirmation, and anyway are useful for other purposes (e.g., granulometry and composition of the particulate material) out of the scope of the present study.

Appendix A

[55] After the dark correction that follows the manufacturer's recommendations has been applied, the residual deep fluorescence signal (say beyond 300 m) is not zero; actually, it remains always positive and differs according to the sensor. *Proctor and Roesler* [2010] have recently studied the effects on the dark count of temperature and of fluorescence by dissolved organic material in shallow freshwaters where this material is extremely abundant, which is never the case here. For all floats except the NAT_IB_B03, the temperature at the parking depth (~1000 m) was rather steady so that a temperature effect on the dark count was never observed. In contrast, the NAT_IB_B03 float has drifted from the Island Basin to the Norwegian Basin, and a large temperature change was observed at ~1000 m, from ~6°C to <0°C. Even under such conditions, the dark current remained unchanged. The average values of the dark signals observed for the various floats are between 0.02 and 0.11 mg m^{-3} when directly expressed in chlorophyll *a* concentration. These values may appear rather high, particularly when considering that for the six floats in oligotrophic environments they are similar to the chlorophyll *a* concentration generally encountered in the upper layers. In terms of digital counts, however, these residual dark signals represent a few counts (2 to 9), to be compared with the dark counts provided by the manufacturer (between 50 and 60 counts) and also with the nominal resolution (equivalent to ~0.03 mg m^{-3}). These last remarks point out that the present fluorimeters are at the limit of their capability when dealing with oligotrophic waters.

[56] **Acknowledgments.** This paper represents a contribution to the remOcean project, funded by the European Research Council, to the PABO project funded by Agence Nationale de la Recherche (ANR), to the BIOSOPE project of the LEFE/CYBER program, and to the BOUSSOLE project. We express our gratitude to Bernard Gentili for help in programming and to John Cullen for helpful suggestions and constructive comments on a first version of this paper. We also would like to thank the NASA Ocean Biology Processing Group (OBPG) for processing and efficient distribution of the MODIS-A data.

References

Althuis, I., W. W. C. Gieskes, L. Villerius, and F. Colijn (1994), Interpretation of fluorometric chlorophyll registrations with algal pigment analysis along a ferry transect in the southern North Sea, *Neth. J. Sea Res.*, *33*(1), 37–46, doi:10.1016/0077-7579(94)90049-3.

Antoine, D., F. d'Ortenzio, S. B. Hooker, G. Bécu, B. Gentili, D. Tailliez, and A. J. Scott (2008), Assessment of uncertainty in the ocean reflectance determined by three satellite ocean color sensors (MERIS, SeaWiFS and MODIS-A) at an offshore site in the Mediterranean Sea (BOUSSOLE project), *J. Geophys. Res.*, *113*, C07013, doi:10.1029/2007JC004472.

Babin, M. (2008), Phytoplankton fluorescence: Theory, current literature and in situ measurements, in *Real-Time Coastal Observing Systems for Marine Ecosystem Dynamics and Harmful Algal Blooms*, edited by M. Babin, C. Roesler, and J. J. Cullen, pp. 237–280, UNESCO, Paris.

Brown, C. A., Y. Huot, M. J. Purcell, J. J. Cullen, and M. R. Lewis (2004), Mapping coastal optical and biogeochemical variability using an autonomous underwater vehicle and a new bio-optical inversion algorithm, *Limnol. Oceanogr. Methods*, *2*, 262–281.

Ciotti, A. M., J. J. Cullen, and M. R. Lewis (1999), A semi-analytical model of the influence of phytoplankton community structure on the relationship between light attenuation and ocean color, *J. Geophys. Res.*, *104*(C1), 1559–1578, doi:10.1029/1998JC900021.

Claustre, H., A. Morel, M. Babin, C. Cailliau, D. Marie, J. C. Marty, D. Tailliez, and D. Vaulot (1999), Variability in particle attenuation and chlorophyll fluorescence in the tropical Pacific: Scales, patterns, and biogeochemical implications, *J. Geophys. Res.*, *104*(C2), 3401–3422, doi:10.1029/98JC01334.

Claustre, H., A. Sciandra, and D. Vaulot (2008), Introduction to the special section: Bio-optical and biogeochemical conditions in the south east Pacific in late 2004: The BIOSOPE program, *Biogeosciences*, *5*, 679–691, doi:10.5194/bg-5-679-2008.

Claustre, H., et al. (2010), Biol.-optical profiling floats as new observational tools for biogeochemical and ecosystem studies, in *Proceedings of the OceanObs'09: Sustained Ocean Observations and Information for Society Conference*, edited by J. Hall, D. E. Harrison, and D. Stammer, *ESA Publ., WPP-306*. (Available at http://www.obs-vlfr.fr/LOV/OMT/fichiers_PDF/Claustre_et_al._OO09.pdf.)

Cullen, J. J., and M. R. Lewis (1995), Biological processes and optical measurements near the sea-surface: Some issues relevant to remote sensing, *J. Geophys. Res.*, *100*(C7), 13,255–13,266, doi:10.1029/95JC00454.

Cunningham, A. (1996), Variability of in vivo chlorophyll fluorescence and its implications for instrument development in bio-optical oceanography, *Sci. Mar.*, *60*, suppl. 1, 309–315.

Falkowski, P., and D. A. Kiefer (1985), Chlorophyll a fluorescence in phytoplankton: Relationship to photosynthesis and biomass, *J. Plankton Res.*, *7*, 715–731, doi:10.1093/plankt/7.5.715.

Fennel, K., and E. Boss (2003), Subsurface maxima of phytoplankton and chlorophyll: Steady-state solutions from a simple model, *Limnol. Oceanogr.*, *48*(4), 1521–1534, doi:10.4319/lo.2003.48.4.1521.

Gordon, H. R. (1989), Can the Lambert-Beer law be applied to the diffuse attenuation coefficient of ocean water?, *Limnol. Oceanogr.*, *34*, 1389–1409, doi:10.4319/lo.1989.34.8.1389.

Gregg, W. W., and K. L. Carder (1990), A simple spectral solar irradiance model for cloudless maritime atmospheres, *Limnol. Oceanogr.*, *35*(8), 1657–1675, doi:10.4319/lo.1990.35.8.1657.

Johnson, K. S., W. M. Berelson, E. S. Boss, Z. Chase, H. Claustre, S. R. Emerson, N. Gruber, A. Körtzinger, M. J. Perry, and S. C. Riser (2009), Observing biogeochemical cycles at global scales with profiling floats and gliders: Prospects for a global array, *Oceanography*, *22*(3), 216–225.

Kiefer, D. A. (1973a), Fluoresence properties of natural phytoplankton populations, *Mar. Biol.*, *22*, 263–269, doi:10.1007/BF00389180.

Kiefer, D. A. (1973b), Chlorophyll *a* fluorescence in marine centric diatoms: Responses of chloroplasts to light and nutrient stress, *Mar. Biol.*, *23*, 39–46, doi:10.1007/BF00394110.

Maritorena, S., A. Morel, and B. Gentili (2000), Determination of the fluorescence quantum yield by oceanic phytoplankton in their natural habitat, *Appl. Opt.*, *39*, 6725–6737, doi:10.1364/AO.39.006725.

Marra, J. (1997), Analysis of diel variability in chlorophyll fluorescence, *J. Mar. Res.*, *55*, 767–784, doi:10.1357/0022240973224274.

Morel, A. (1988), Optical modeling of the upper ocean in relation to its biogenous matter content (case I waters), *J. Geophys. Res.*, *93*(C9), 10,749–10,768, doi:10.1029/JC093iC09p10749.

Morel, A., and B. Gentili (2009), The dissolved yellow substance and the shades of blue in the Mediterranean Sea, *Biogeosciences*, *6*, 2625–2636, doi:10.5194/bg-6-2625-2009.

Morel, A., and S. Maritorena (2001), Bio-optical properties of oceanic waters: A reappraisal, *J. Geophys. Res.*, *106*(C4), 7163–7180, doi:10.1029/2000JC000319.

Morel, A., H. Claustre, D. Antoine, and B. Gentili (2007a), Natural variability of bio-optical properties in case 1 waters: Attenuation and reflectance within the visible and near-UV spectral domains, as observed

in South Pacific and Mediterranean waters, *Biogeosciences*, *4*, 913–925, doi:10.5194/bg-4-913-2007.

Morel, A., Y. Huot, B. Gentili, P. J. Werdell, S. B. Hooker, and B. A. Franz (2007b), Examining the consistency of products derived from various ocean color sensors in open ocean (case 1) waters in the perspective of a multi-sensor approach, *Remote Sens. Environ.*, *111*, 69–88, doi:10.1016/j.rse.2007.03.012.

Morrison, J. R. (2003), In situ determination of the quantum yield of phytoplankton chlorophyll a fluorescence: A simple algorithm, observations, and a model, *Limnol. Oceanogr.*, *48*(2), 618–631, doi:10.4319/lo.2003.48.2.0618.

Nahorniak, J. S., M. R. Abbott, R. M. Letelier, and W. S. Pegau (2001), Analysis of a method to estimate chlorophyll-*a* concentration from irradiance measurements at varying depths, *J. Atmos. Oceanic Technol.*, *18*, 2063–2073, doi:10.1175/1520-0426(2001)018<2063:AOAMTE>2.0.CO;2.

O'Reilly, J. E., et al. (2000), Ocean color chlorophyll a algorithms for SeaWiFS, OC2, and OC4: Version 4, SeaWiFS postlaunch calibration and validation analyses, Part 3, *NASA Tech. Memo., TM-206892*, vol. 11, 9–23.

O'Reilly, J. E., S. Maritorena, B. G. Mitchell, D. A. Siegel, K. L. Carder, S. A. Garver, M. Kahru, and C. McClain (1998), Ocean color chlorophyll algorithms for SeaWiFS, *J. Geophys. Res.*, *103*(C11), 24,937–24,953, doi:10.1029/98JC02160.

Proctor, C. W., and C. S. Roesler (2010), New insights on obtaining phytoplankton concentration and composition from in situ multispectral chlorophyll fluorescence, *Limnol. Oceanogr. Methods*, *8*, 695–708, doi:10.4319/lom.2010.8.695.

Ras, J., H. Claustre, and J. Uitz (2008), Spatial variability of phytoplankton pigment distributions in the subtropical South Pacific Ocean: Comparison between in situ and predicted data, *Biogeosciences*, *5*(2), 353–369, doi:10.5194/bg-5-353-2008.

Sackmann, B. S., M. J. Perry, and C. C. Eriksen (2008), Seaglider observations of variability in daytime fluorescence quenching of chlorophyll-*a* in northeastern Pacific coastal waters, *Biogeosciences Discuss.*, *5*, 2839–2865, doi:10.5194/bgd-5-2839-2008.

Zaneveld, J. R. V., E. Boss, and A. Barnard (2001), Influence of surface waves on measured and modeled irradiance profiles, *Appl. Opt.*, *40*(9), 1442–1449, doi:10.1364/AO.40.001442.

D. Antoine, H. Claustre, F. D'Ortenzio, A. Mignot, A. Morel, A. Poteau, and X. Xing, Laboratoire d'Océanographie de Villefranche, Marine Optics and Remote Sensing Lab, BP 8, Quai de la Darse, F-06230 Villefranche-sur-Mer, France. (xingxiaogang@obs-vlfr.fr)